Results in Engineering 29 (2026) 108961

Contents lists available at ScienceDirect

Results in Engineering

journal homepage: www.sciencedirect.com/journal/results-in-engineering

Research paper

The pivotal role of particle size on REE enrichment and extraction efficiency: A multi-modal characterization and leaching study of bastnäsite ore

S. Samet Kaplan [a,b], Cisem Celik-Kurtulan [a,c], Elif Emil-Kaya [d,*], Gabriella Tranell [d], M. Seref Sonmez [a]

[a] Department of Metallurgical and Materials Engineering, Faculty of Chemical and Metallurgical Engineering, Istanbul Technical University, Sarıyer, Istanbul, Türkiye
[b] Department of Metallurgical and Materials Engineering, Faculty of Engineering & Natural Sciences, Hitit University, Çorum, Türkiye
[c] Rare Earth Elements Research Institute, Turkish Energy, Nuclear and Mineral Research Agency, Kahramankazan, Ankara, Türkiye
[d] Department of Materials Science and Engineering, Norwegian University of Science and Technology, 7491, Trondheim, Norway

ARTICLE INFO

Keywords:
Automated mineralogy
Rare earth elements
Bastnäsite
Eskisehir-kizilcaoren deposit
Critical minerals

ABSTRACT

A detailed multi-modal characterization and extraction investigation was performed on bastnäsite ore from Türkiye's Kızılcaören deposit to elucidate REE enrichment mechanisms across different particle sizes. The as-received ore was fractionated and rigorously analyzed using Automated Mineralogy (AM), ICP-MS, and XRD. Results revealed a strong dependency of REE concentration on particle size, particularly below 40 μm. Light REE content quadrupled from 2.5 wt.% (±0.83) to 10.6 wt.% (±3.00), while Heavy REE increased from 835.7 ppm (±346.33) to 3867.5 ppm (±1056.9), with high standard deviations suggesting uneven elemental distribution. Consistent with chemical data, AM analysis showed that the area occupied by REE minerals (bastnäsite, monazite, parisite, synchysite) increased from 2.6% to 3.8% in fractions <40 μm. Mineralogical mapping highlighted strong associations between REE phases and barite/Fe-Mn oxides rather than the primary fluorite phase. Furthermore, Rietveld refinement confirmed that bastnäsite content rose from 3.8 wt.% to 9.5 wt.% in fine fractions. Leaching experiments in two different acidic media indicated no significant performance difference; however, the finest fraction (<25 μm) yielded the highest extraction concentrations (1215 ppm Ce, 1062 ppm La, 134.3 ppm Nd). This study demonstrates that particle size is the paramount factor governing REE enrichment and hydrometallurgical extraction, providing critical data for optimizing pre-concentration and leaching flowsheets.

1. Introduction

The 21st century's fundamental transition to a circular economy is intrinsically linked to the rapid electrification of transport and the proliferation of high-tech devices. Rare Earth Elements (REE) are at the core of these technological shifts. Due to their indispensable role in achieving sustainability and climate goals, REE have been designated by the European Commission as minerals posing the highest supply risk [1]. This criticality underscores the urgent need not only to secure new sources but also to optimize the beneficiation efficiency of complex, low-grade ores globally.

Currently, carbonatite-hosted deposits represent the world's primary source of Light REE (LREE). China continues to dominate this landscape with the Bayan Obo deposit, holding the largest stockpile of 44 million metric tons and over 60 % of global production [2–5]. Similarly, in the Western hemisphere, the USA produced 45,000 t in 2024, sourced entirely from the carbonatite-hosted Mountain Pass deposit [6]. Other significant reserves include Brazil's Araxá deposit (6.34 million tons REO) [7], the Morro dos Seis Lagos deposit in the Amazon [8], and Vietnam's Dong Pao and Nam Xe deposits [9–11].

While carbonate-based minerals remain the dominant global sources, the intensifying demand has prompted the exploration of alternative geological settings. Ion-adsorption clays (IACs), predominantly found in South China, represent a pivotal category, supplying the majority of the world's Heavy REE (HREE) through adsorption onto fine-grained aluminosilicates [12,13]. Concurrently, coal deposits and coal combustion by-products (fly ash) have emerged as promising unconventional sources [14,15]. Research indicates that REEs in these materials are often

* Corresponding author.
E-mail addresses: ssametkaplan@hitit.edu.tr (S.S. Kaplan), elif.e.kaya@ntnu.no (E. Emil-Kaya).

https://doi.org/10.1016/j.rineng.2026.108961
Received 3 November 2025; Received in revised form 28 December 2025; Accepted 1 January 2026
Available online 2 January 2026

encapsulated within fine-grained glassy phases or associated with clay minerals, requiring advanced characterization to unlock their potential [16]. In addition, sedimentary phosphorites have gained attention; for instance, phosphorites in India were reported to contain REE enrichments up to 1075 ppm [17]. Crucially, characterization studies on these deposits consistently emphasize the importance of grain size distribution. Although statistical analysis of various fractions in Tebessa (Algeria) phosphorites initially suggested a homogenous distribution [18], targeted investigations revealed distinct enrichment in the fine-grained matrix (<45 μm) with REY (REE+Y) values reaching 863 ppm [19].

Within this global context, Türkiye possesses four major REE deposits, with the Eskişehir-Kızılcaören deposit being the most significant. It is a complex carbonatite-hosted fluorite-barite-REE deposit, and at the time of discovery 1977 its reserve was estimated at 0.2 % ThO_2 and nearly 3 % of REE (Ce, La, Nd, Y). In addition, it was noted that the field has more potential than discovered at the time [20]. Detailed studies by Gültekin et al. divided the Kızılcaören deposit into four districts: Kocayayla, Yaylabaşı, Höyüklü, and Devebağırtan. High-grade ore bodies in Devebağırtan are entirely within triassic metasedimentary rocks, while mineralization in other areas occurs in vuggy and massive silica bodies within breccia zones. Key REE-bearing minerals are reported as bastnäsite ($CeCO_3F$), brockite ($CaTh[PO_4]_2{\cdot}H_2O$), fluocerite ($CeAl_3[(OH)_6/(PO_4)_2]$), and monazite ($CePO_4$) [21,22]. Similar mineral composition was also reported by different authors [23,24]. However, metallurgical efficiency remains a challenge due to the complex mineralogy. Previous studies have attempted various beneficiation routes. Turker G. et al. (2023) reported that a grinding-classification method increased REO concentration from 3 % to 13.25 % but noted significant dependency on particle size [25]. Another study further identified bastnäsite, monazite, cerianite, and lateritic minerals as the primary REE carriers consisting of 6.9 wt. % within the +25 μm to −150 μm particle size range [26]. Similarly, Yeşilören-Görmüş et al. (2021) and Baştürkcü et al. (2022) utilized Mineral Liberation Analysis (MLA) to identify mineral phases, noting that mechanical attrition could redistribute REE into finer fractions [27,28].

Despite these valuable contributions, a comprehensive, size-by-size process mineralogy characterization of a representative run-of-mine feed is lacking. Most prior studies focus on geological descriptions or specific concentration tests, leaving a gap in understanding the fundamental natural fractionation of REE during the initial comminution stages. Herein, we present the first detailed, systematic characterization of the Kızılcaören ore across nine distinct particle size fractions to precisely determine the distribution and enrichment behavior of REE depending on particle size. Adopting a modern geometallurgical approach, a powerful combination of Automated Mineralogy (AM), ICP-MS, and quantitative Rietveld refinement of XRD data was utilized to conclusively map the REE-rich particle size distribution and confirm the dominant REE-bearing phases. Finally, leaching studies were conducted on the calcined fractions to establish a direct correlation between optimized particle size and maximum REE leaching efficiency. This study demonstrates that particle size is the paramount factor governing REE enrichment in Kızılcaören and establishes a reproducible framework for optimizing the processing of similar complex bastnäsite-type ores globally.

2. Experimental

2.1. Characterization

The ore sample from Eskişehir-Kızılcaören REE deposit was kindly supplied by Türkiye Energy, Nuclear and Mine Research Institution – Rare Earth Elements Research Institute (TENMAK-NATEN). To determine the particle size distribution, and other characteristics (like chemical content, phase analysis) of the supplied ore, a 300 g representative sample was obtained from the initial 25 kg of ore using the quartering method, and then subjected to wet sieve analysis. After the sieving, particles in each screen openings were grinded in agate mortar for homogenization and further characterization.

2.2. Chemical analysis

Light, heavy REE, Th, and U totally 19 elements' content throughout whole particle size ranges was determined by ICP-MS analysis using Thermo-Scientific X-Series-II equipment. To ensure representativeness, 3 different solid samples were analyzed from each screen. These samples were digested by using sodium peroxide digestion method which was used as in another study [29]. The instrument was calibrated by using certified reference solution supplied by inorganic ventures company yielding calibration curves with a correlation coefficient (R^2) greater than 0.998. To ensure the accuracy, recovery rate for the solution with a known concentration was found to be within the range of 95–105 %, and internal standard element was also used to ensure the plasma stability during the analysis which gives acceptable recovery rates between 90–110 %.

The overall REE content of the sample was calculated as a mass-weighted average, utilizing the mass fraction and chemical composition of each size fraction obtained from sieve analysis. The average concentration of each element, and standard deviation were calculated by following Eqs. (1), and 2, respectively. In equations, $\overline{C}_{REE}$ is calculated mass-weighted average REE concentration, w_i is the mass fraction of the material in i th sieve interval, C_i is the measured REE concentration in i th sieve interval, n is the total number of sieve fractions, and SD_w is standard deviation.

$$\overline{C}_{REE} = \sum_{i=1}^{n} \left(w_i . C_i \right) \tag{1}$$

$$SD_w = \sqrt{\sum_{i=1}^{n} w_i (C_i - \overline{C}_{REE})^2} \tag{2}$$

2.3. Phase and mineralogical analysis

For the determination of phases, XRD analysis were conducted between 10°−90° with a scanning rate of 2°/min with Cu Kα (λ = 1.5406 Å). XRD patterns of all powders left between each sieve openings had different intensities, and they were normalized to obtain accurate, and comparable results. Also, Rietveld analysis was conducted to understand phase distribution in terms of REE bearing mineral content for each screen. SEM-EDS analysis (FEI-Quanta FEG 250) was also conducted to understand the chemical composition, and morphology of each phase. Ore particles below 40 μm were used for SEM-EDS analysis as mounted in epoxy resin. The sample was polished, and coated with Au to avoid charging in SEM.

Three representative samples with different particle sizes, from fine to coarse, were selected for automated mineralogy (AM) analysis. A photograph of the samples placed in the sample holder is shown in Fig. 1. For samples A and B (referred to as Bast-A and Bast-B, respectively), representative areas were scanned, whereas for sample C (Bast-C), the entire sample was scanned due to its small grain size. All samples were analyzed using scanning electron microscope-based automated mineralogy (SEM-AM) with a ZEISS Sigma 300VP field emission SEM. The system was equipped with two Bruker Xflash 6|60 (GEUS: 6|30) 129 eV energy dispersive X-ray spectroscopy (EDS) detectors, as well as backscattered electron (BSE) and secondary electron (SE) detectors. Samples were prepared as polished, carbon-coated epoxy pucks before analysis, and the raw data were processed accordingly.

For AM analysis, EDS spectra were systematically collected using ZEISS Mineralogic, covering a high-resolution grid across the analyzed grains. Each individual EDS spectrum was quantified, enabling the classification of mineral or chemical phases based on elemental

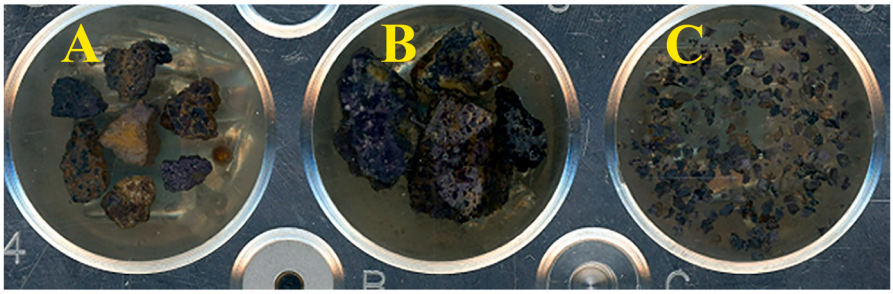

Fig. 1. Samples mounted in SEM holder for mineralogical analysis.

composition (wt. %) as defined in a mineral list. The step size of the high-resolution EDS grid is flexible, ranging from a few hundred nanometers to tens of micrometers. It is user-defined and typically selected based on grain size and research objectives.

In this study, a step size of 4 μm was chosen to detect various minerals while minimizing the effects of beam interaction with the sample material. The acceleration energy was set to 15 kV, with a working distance of 8.5 mm and a 120 μm aperture. For each analyzed sample area, mineral and BSE maps were generated, along with data tables providing quantitative modal mineralogy (bulk mineralogy), mineral associations, and element assays. Mineral and phase identification was carried out through both manual and automated SEM-EDS microanalysis of various ore components. The resulting mineralogical data were visualized as false-color mineral maps overlaid on backscattered electron (BSE) micrographs.

2.4. Leaching

Prior to leaching experiments, the bastnäsite ore was calcined at 500 °C during 8 h which optimized in a previous study [29]. The processed ore, broken down into different particle sizes, was then leached with two types of acids—nitric acid (HNO_3) and sulfuric acid (H_2SO_4)—to figure out the best particle size for efficient processing. Since the main goal was to identify the ideal particle size range for processing the ore, 4 different particle size ranges below 355 μm were selected, other parameters were kept constant which are temperature (60 °C), solid/liquid ratio (1/40), molarity (2 mol/L), and duration (4 h). Leaching experiments were carried out in a setup consisting of three-necked round-bottom flasks placed in a silicone oil bath. The solutions within the flasks were mechanically stirred at 300 rpm using an overhead stirrer. The oil bath was placed on a heating plate, and temperature was controlled thorough thermocouple immersed into solution through one of the flask necks. A condenser, also connected to a flask neck, was used to prevent solution evaporation.

3. Results and discussion

3.1. Sieve analysis

Initially, as received ore was subjected to wet sieve analysis. Particle size distribution graph is given in Fig. 2. According to results, 97 wt. % of the ore was below 5 mm, and 20.7 wt. % was below 40 μm. D_{50} was found to be 0.362 mm. From C_c (28.14), and C_u (1.01) value, it can be said the analyzed ore is poorly graded. This is because no grinding was applied to as obtained ore.

3.2. Chemical analysis

The chemical analysis of 17 REE, Th, and U was conducted across nine particle size ranges with the complete Ndataset provided in Supplementary Tables S.1, and S.2. The distribution of the most concentrated elements is visualized as a heatmap in Fig. 3. The data clearly indicate that REE are significantly enriched in the finer particle fractions. This trend is driven primarily by La and Ce (LREE), Gd and Y (HREE), and Th.

Quantitative results show that the total LREE concentration increases from 2.66 wt. % in the coarse fraction (>25 μm) to 12.23 wt. % in the fine fraction (<25 μm). Similarly, the total HREE concentration exhibits a sharp increase, reaching 4450.56 ppm in the <25 μm fraction. Overall, both LREE and HREE concentrations show an approximate six-fold increase in the finest fraction compared to the coarse material.

The mass-weighted average concentrations calculated from Eq. (1) for the major elements were determined as 1.77 wt. % for La, 1.98 wt. % for Ce, and 0.29 wt. % for Nd (Table 1). Most of elements' distribution is more uniform above 40 μm in comparison to finer particles. However, as detailed in the table, the standard deviations relative to general means are notably high. This statistical variance confirms a significant heterogeneity in elemental distribution across particle sizes. This phenomenon is most pronounced for Th which exhibits the highest deviation from the mean, suggesting its strong preferential accumulation in specific, fine-grained size ranges.

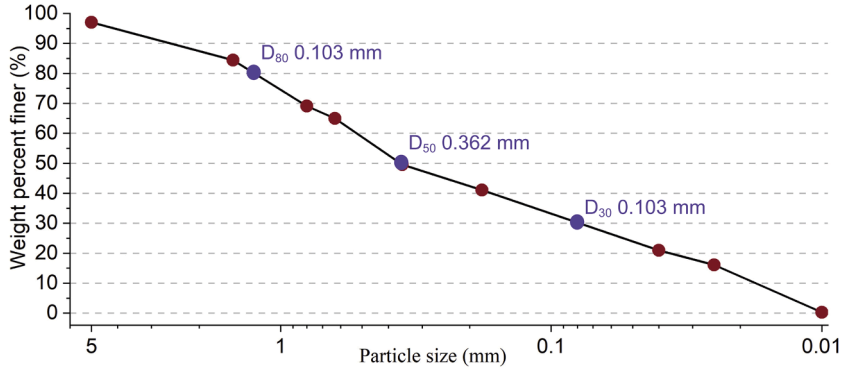

Fig. 2. Particle size distribution of as received bastnäsite ore.

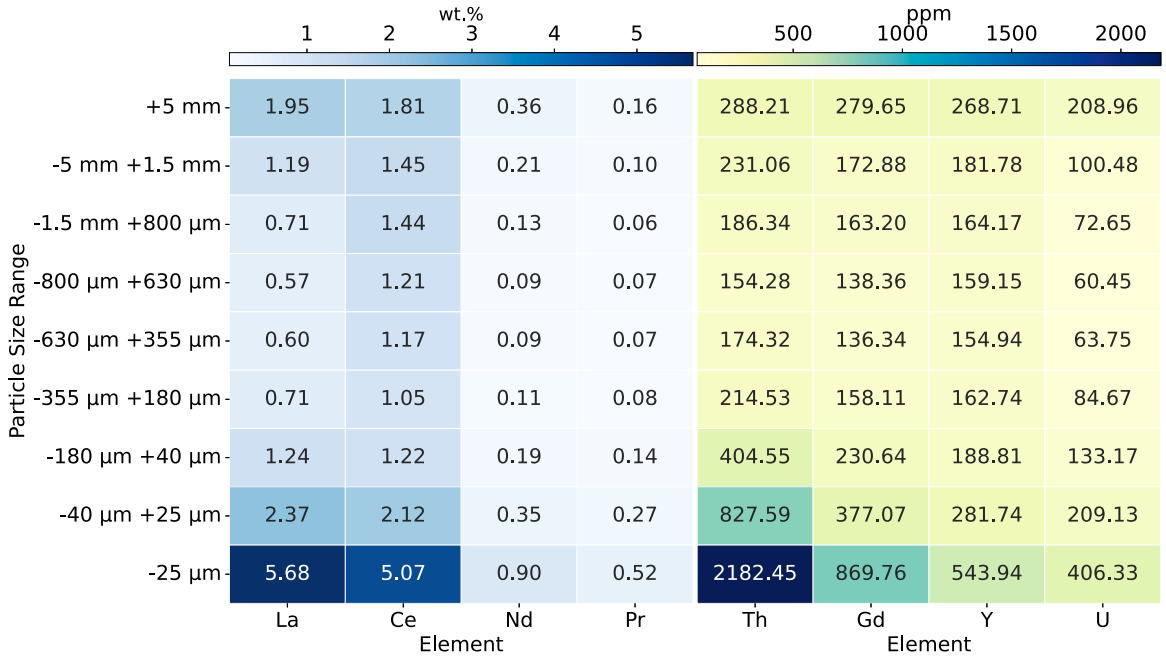

Fig. 3. Distribution of REE through different particle size ranges (exact values are given in supplementary Table S.1).

Table 1
Average REE, Th, U concentrations in Eskişehir bastnäsite ore defined by ICP-MS.

Element	La (wt. %)	Ce (wt. %)	Nd (wt. %)	Pr (wt. %)	Sm (wt. %)	Th (ppm)	Gd (ppm)	Y (ppm)	U (ppm)
Conc.	1.77 (± 1.77)	1.94 (±1.39)	0.28 (±0.28)	0.17 (±0.16)	0.02 (±0.02)	590.92 (±712.90)	300.12 (±255.62)	239.63 (±136.77)	151.97 (±118.19)
Element	Eu (ppm)	Dy (ppm)	Er (ppm)	Yb (ppm)	Tb (ppm)	*Sc* (ppm)	Ho (ppm)	Tm (ppm)	Lu (ppm)
Conc.	69.74 (±37.40)	40.92 (±33.16)	24.89 (±18.97)	17.42 (±11.83)	14.61 (±12.21)	8.75 (±5.70)	7.57 (±5.47)	3.18 (±2.03)	2.67 (±1.69)

3.3. Automated mineralogy analysis

The mapping analysis for Samples A and B, which primarily consist of coarser particles, is illustrated in Fig. 4. In contrast, Fig. 5 presents a part of whole mineral mapping image, and mineral occupancy area percentages for Sample C, which mainly contains finer particles. Whole BSE, and colored mineral image of sample C is given in Figure S.1. The minerals in the graphs are categorized into main, minor, and REE-bearing minerals to enhance clarity and readability of graphs. Additionally, the area occupancy values for all detected minerals are listed in Table S.3.

Fluorite and barite were identified as the dominant phases occupying approximately 65 % and 10 % of the scanned area, respectively, across all particle size ranges. These two phases are generally found as barite distributed through fluorite matrix as illustrated in Fig. 5. Mn-oxide and Fe-oxide minerals were also detected as significant secondary phases; however, their distribution was inconsistent across different particle sizes. For instance, Fe-oxide accounted for around 10 % in the Bast-A sample but dropped to <1 % in the Bast-B sample, a difference visually corroborated by the brown area in the photograph of the sample A (Fig. 1). Similarly, Mn-oxide minerals exhibited random and uneven distribution patterns throughout the analyzed samples. These differences in Fe-oxide, and Mn-oxide percentages indicate that their distribution across the received ore sample is non-uniform.

Among the various REE-bearing minerals identified, including bastnäsite, monazite, parisite, and synchysite, bastnäsite was the most prevalent. Mineralogical mapping further revealed that REE-bearing minerals, particularly bastnäsite, were more frequently associated with barite, iron oxides, and manganese oxides than with fluorite, the primary mineral phase. Based on Automated Mineralogy (AM) results, the distribution of REE increased as particle size decreased (from Bast-A sample to Bast-C sample in Table S.3), which aligns with the findings from chemical analysis. The enrichment of REE in fine fractions especially below 25 µm is primarily attributed to the inherent textural characteristics of the ore. AM analyses reveal that bastnäsite occurs as naturally fine-grained disseminations within the ore matrix. Consequently, upon liberation—whether through natural breakage or comminution—bastnäsite minerals preferentially accumulate in the finest fractions.

3.4. Phase analysis

To determine the phase composition and crystalline structure variance across whole particle size ranges, nine separate X-ray diffraction patterns were collected, one from each powder fraction. It was concluded that the ore mainly was composed of fluorite (CaF_2), barite ($BaSO_4$), fluor-phlogopite ($KMg_3Si_3AlO_{10}F_2$), calcite ($CaCO_3$), bastnäsite ($LnCO_3F$), and monazite ($LnPO_4$) as can be seen from the Fig. 6 showing a comparative analysis of XRD patterns obtained from 9 distinct particle size fractions. In this figure, main phases were shown for clear comparison, and also detailed labelled patterns figure is given in supplementary file (Figure S.2) Major phases as detected from AM analysis are the same for XRD analysis. Despite a thorough search of various databases, certain minerals identified through AM, such as Mn-oxides and Fe-oxides, could not be clearly indexed in the diffraction patterns. The reason why Fe compound in the ore could not be detected might be due to Cu Kα radiation interferences with Fe fluorescence. Besides, the XRD analysis revealed the presence of fluor-phlogopite, a mineral previously

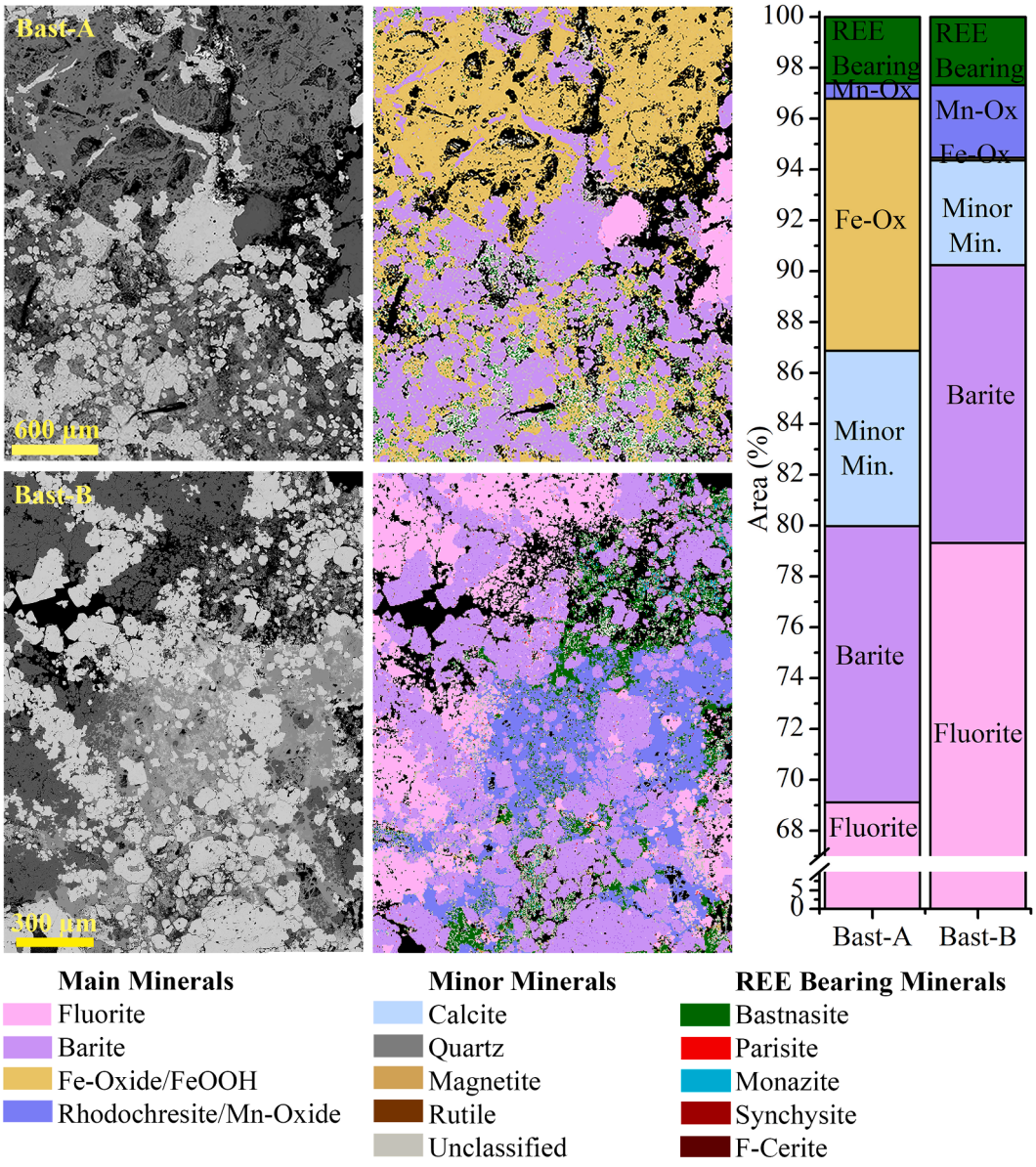

Fig. 4. BSE image, and mineralogical mapping of coarser particles showing REE minerals concentrated areas.

suggested by Gültekin et al., 2003. Its diffraction peaks become quite strong in +355 μm −630 μm sieve portions, and in this portion REE concentration was the lowest (Fig. 3). EDS line analysis result showing an increase in fluor-phlogopite phase elements (Mg, Al, Si, and K) is given in Figure S.3. Although EDS, and AM analyses were performed on the same Bast-C sample, the fluor-phlogopite phase, whose chemical composition was clearly identified in the EDS line analysis, could not be indexed in the AM analysis. The observed discrepancy could be attributed to the random distribution of minerals within the sample. Additionally, a mismatch in stoichiometry may have led to the fluor-phlogopite phase being categorized as undefined phase which constitutes of 4 % of total sample (Table S.3). Minor phases like calcite detected from mineralogical mapping was found as distributed in XRD patterns throughout different particle size ranges. The strongest peak of calcite (ICSD: 98–003–5029) is at 29.41°, and this was clearly detected in + 1.5 mm – 1.5 mm sieve portion, while in other screens whether it is quite weak or absent. For REE-bearing minerals, the bastnäsite peak became increasingly distinct, particularly in the last three sieve fractions, where its content tripled, as confirmed by chemical analysis. Additionally, a weak monazite peak began to appear, which is expected given its low concentration. Although Ca was detected in EDS chemical analysis in REE rich area (Fig. 7), Ca containing REE phases like synchysite, and parisite could not be observed from XRD patterns, and scarcely detected in AM results. According to Yunxiang Ni et al., during geological evaluations, Ca layers contacting two bastnäsite layers were not stable, and those layers transformed to vaterite ($CaCO_3$) phase rather creating long synchysite, and parisite minerals [30]. These vaterite layers possibly formed between bastnäsite layers in the ore were quite thin to be detected by XRD analysis, and Ca amount found in REE rich area stoichiometrically is not enough to create Ca containing REE minerals. Eventually, main REE bearing mineral in the ore from Eskişehir-Kızılcaören province was found to be bastnäsite.

For evaluation of XRD, AM data collaboratively, they are largely in agreement regarding the main and rare earth element (REE)-bearing minerals while their results may initially appear inconsistent for minor phases. The discrepancies observed in the identification of minor minerals, which constitute <6 % of the ore, are not unusual in mineralogical studies and highlight the difficulties in accurately characterizing low-abundance mineral components.

Following phase determination, Rietveld analysis was conducted.

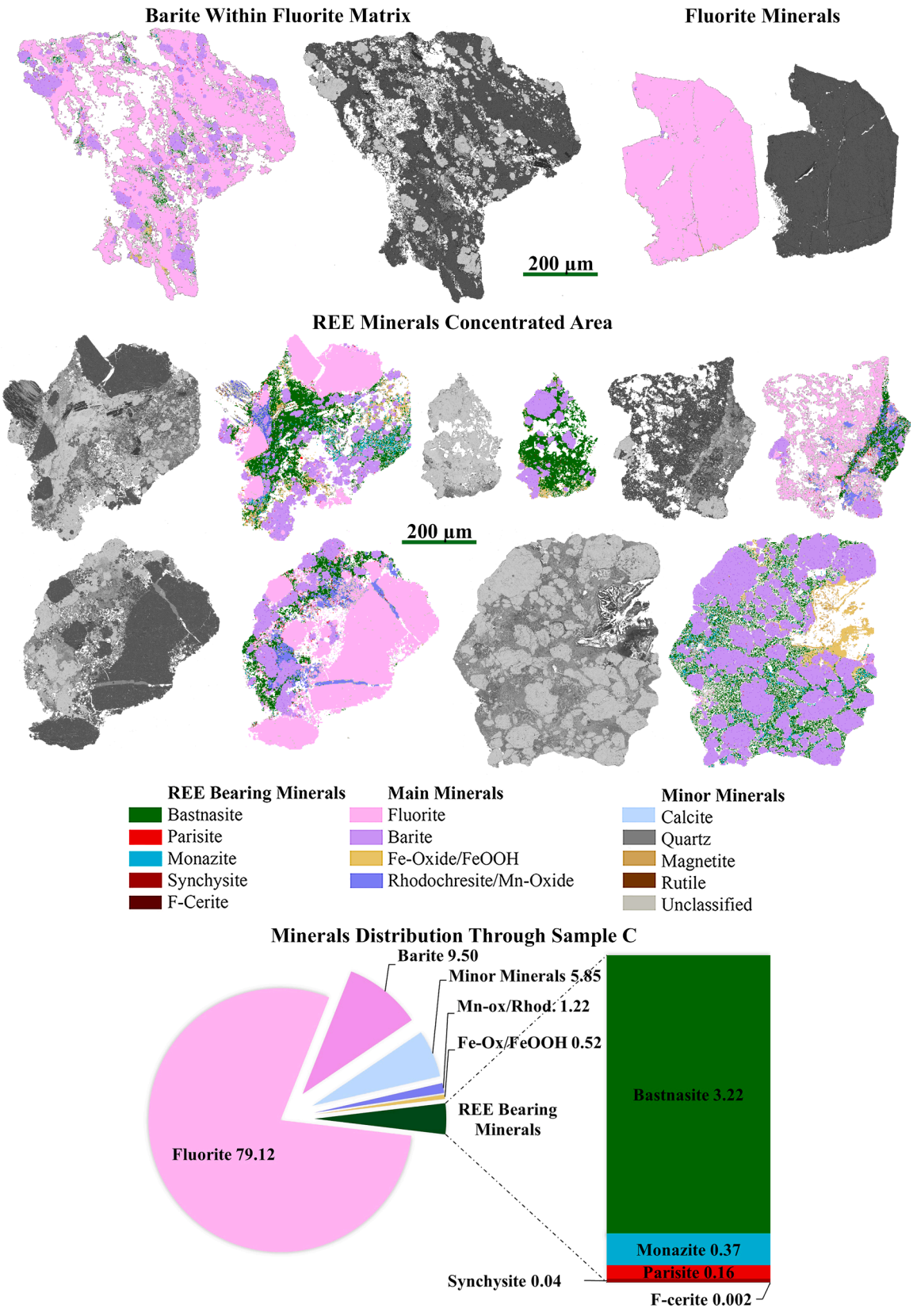

Fig. 5. BSE image, and mineralogical mapping of finer particles showing REE minerals concentrated areas.

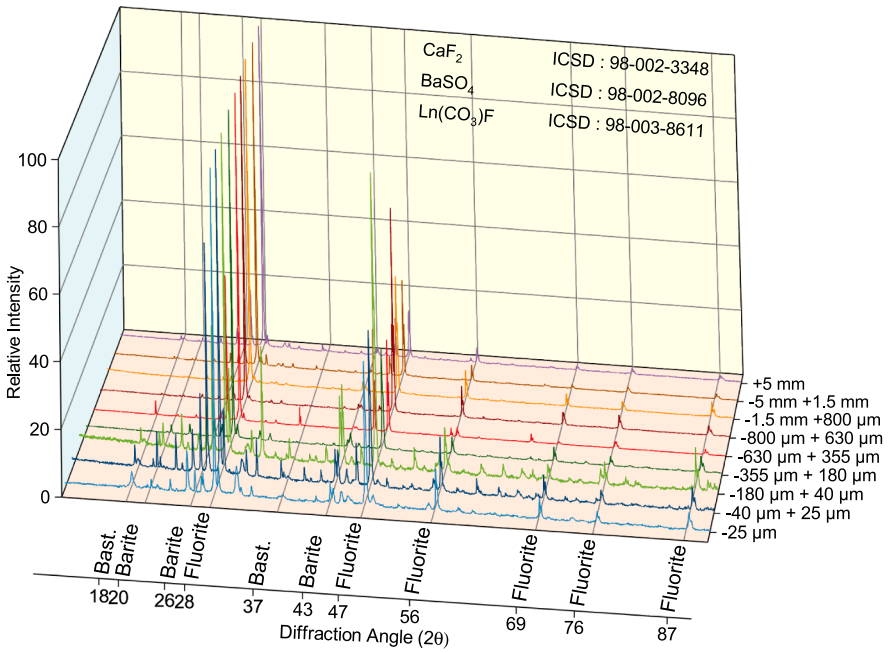

Fig. 6. XRD analysis of the ore for each sieve ranges.

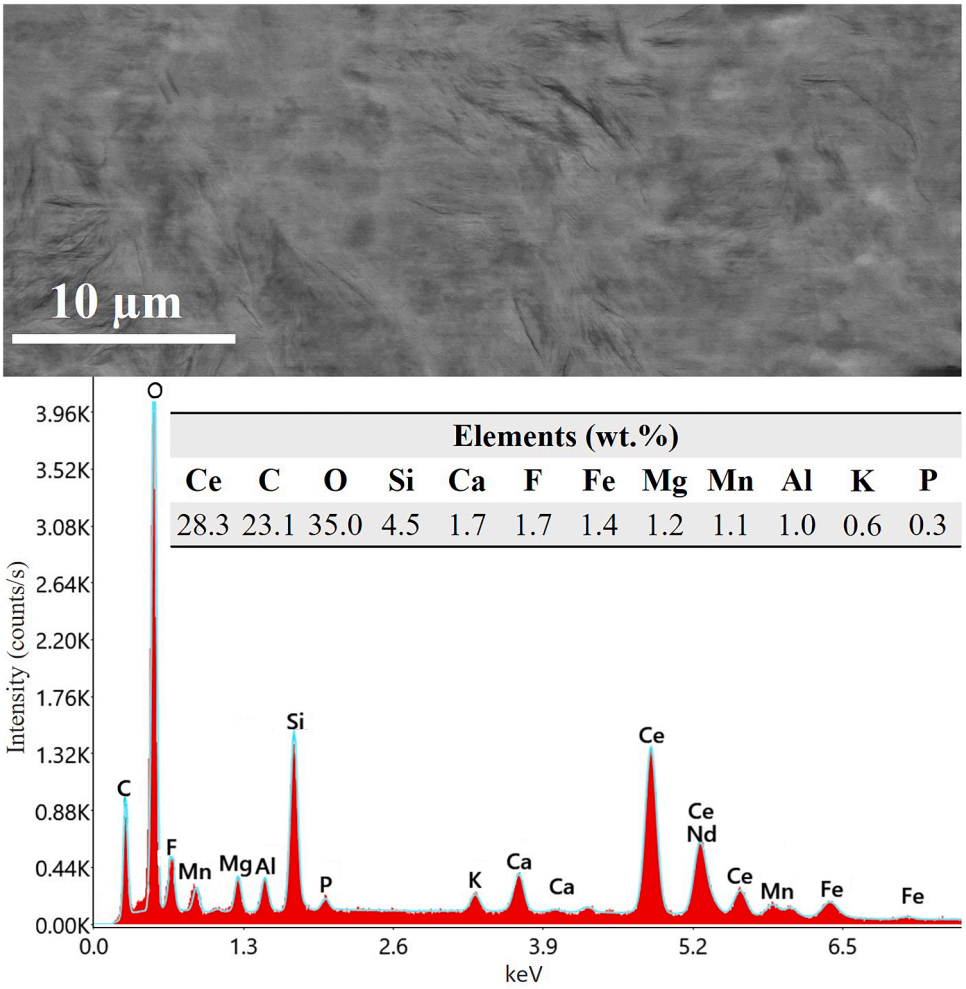

Fig. 7. EDS analysis of REE rich area in Bast-C sample.

XRD patterns of final three sieve openings, and calculated phase compositions of detected phases as weight percentages (expressed in pie charts) are given in Fig. 8. All fitting parameters like goodness of fit, R-expected values are given in supplementary data (Table S.4). Those parameters were within the acceptable ranges proving that data was accurate. It was clear that bastnäsite, and monazite contents were in an increasing manner with a decreasing particle size. Their content was almost tripled below 40 μm particle size. Bastnäsite increased from 3.8 wt. % to 9 wt. %, and monazite increased from 0.1 wt. % to 3.3 wt. %. This result is in a good agreement with the chemical analysis. According to difference plots given in Fig. 8, main differences between calculated, and observed data were due to the barite, and fluorite phase mismatches. This difference was expected coming from some impurity elements dissolved in these phases or crystal growth direction during the geological evolution. According to SEM-EDS analysis given in Fig. 9A, it was understood that Mn has been found as an impurity element in CaF_2, and in Fig. 9B, Si has been found as an impurity element in barite phase. These impurity elements might be the main reason behind the shift in XRD patterns found as a result of Rietveld analysis given in Fig. 8.

3.5. Leaching

Calcines with varying particle size distributions and corresponding differences in REE content were leached using two different media HNO_3, and H_2SO_4. All leaching parameters were kept constant across experiments with only the leaching medium and particle size range being varied. The resulting leachate concentrations are presented in Fig. 10. As evident from the figure, the highest leachate concentration was obtained from calcines with particles smaller than 25 μm whereas lowest concentrated solution was obtained at +180 μm −355 μm. Relative element concentrations are similar to the ore as Ce, and La have the highest concentrations whereas Nd was found to be one-third-of them. Mineralogical mapping (Fig. 4) indicates that REE minerals in coarser fractions are largely interlocked with the gangue minerals, hindering acid attack. In contrast, the finer fractions (Fig. 5) are characterized by liberated REE phases. Consequently, the combination of enhanced mineral accessibility and increased specific surface area led to the maximized REE concentrations in the leachate. Even against the slightly higher LREE-concentrated solution obtained from nitric acid leaching, the final LREE concentration in both acidic media was quite

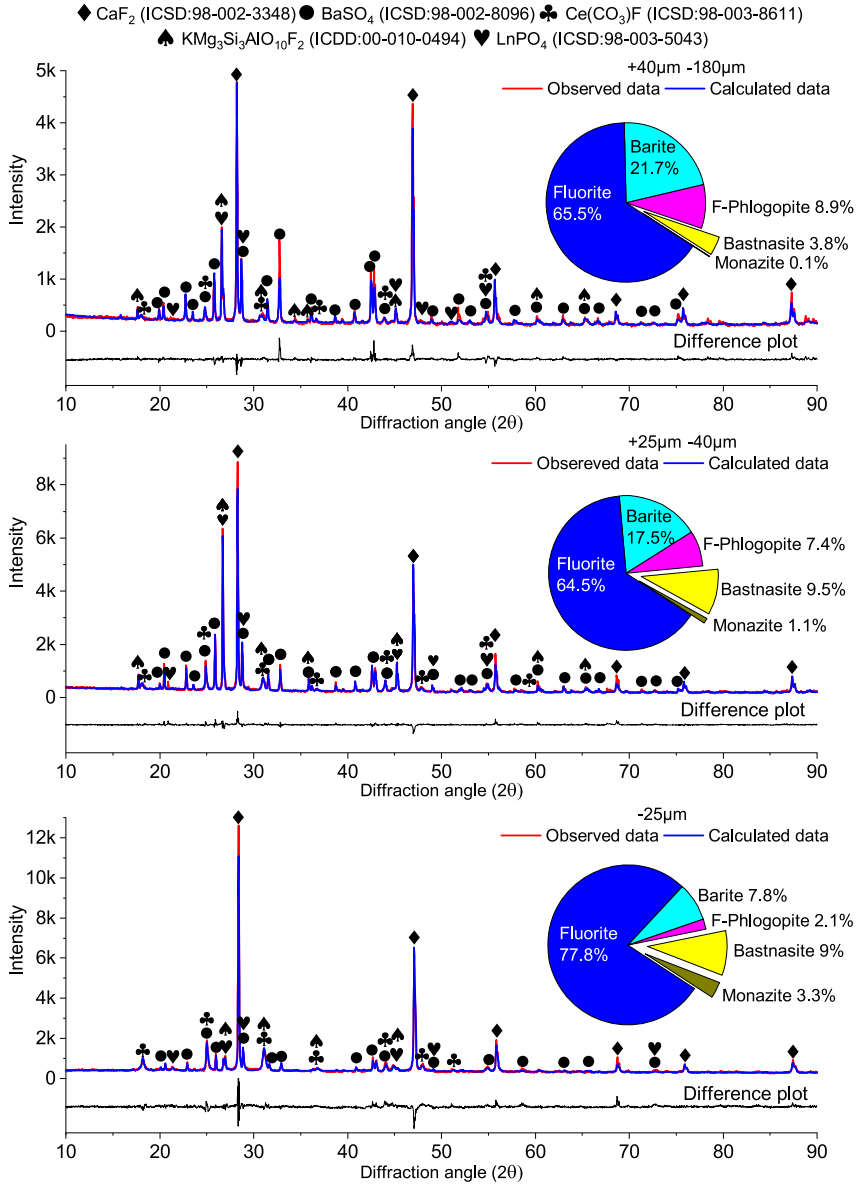

Fig. 8. Rietveld analysis of ore particles within the range of +40 −180 μm, +25 μm −40 μm, −25 μm.

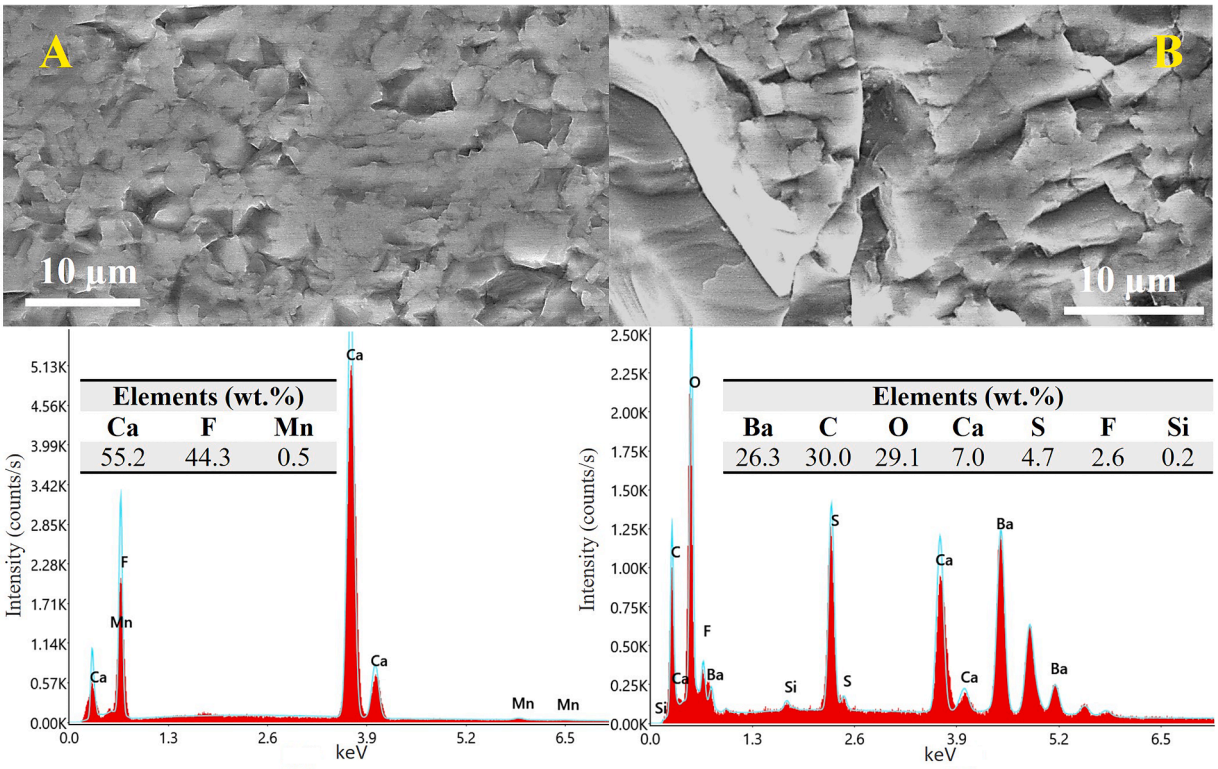

Fig. 9. SEM-EDS analysis of A) fluorite, B) barite minerals.

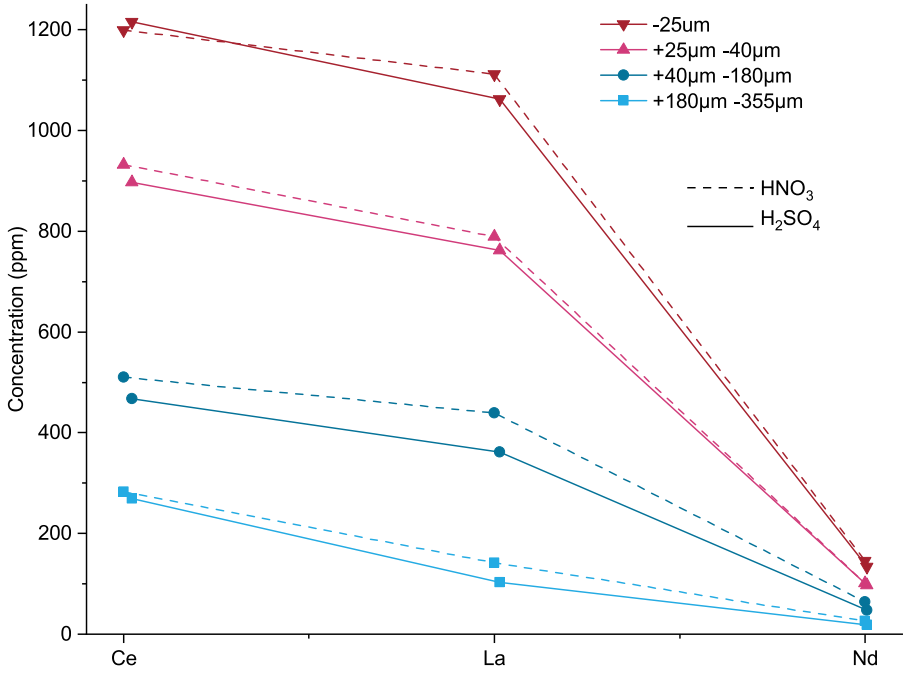

Fig. 10. The comparison of Ce, La, Nd concentration depending on leaching media, and ore particle size ranges (Constant leaching conditions: 60 °C temperature, 1/40 solid/liquid ratio, 2 mol/L acid concentration, and 4 h duration).

similar, indicating that the choice of leaching medium has a minimal impact on leaching efficiency.

4. Conclusion

This comprehensive investigation successfully assessed the critical influence of particle size on the distribution, enrichment, and hydrometallurgical recovery of REE from the Eskişehir-Kızılcaören bastnäsite ore, Türkiye's most significant REE resource. By employing a rigorous, multi-modal characterization approach across nine distinct size fractions, the study yielded crucial data for optimizing the processing flowsheet of this complex ore.

The chemical analysis, covering 17 individual REEs plus Th and U, definitively showed that REE content is inversely proportional to

particle size. The average LREE content in the overall ore was determined to be 4.2 wt. % (± 3.6), while the total HREE concentration, including Th and U, reached 1472.4 ppm (± 1341.3). Crucially, the total concentrations of both LREE, and HREE quadrupled in the finest fraction (below 40 μm) compared to the coarser material, confirming the three finest particle size fractions (below 180 μm) as the primary zone of enrichment. This increasing REE content in finer particles was directly correlated with phase analysis, as both Automated Mineralogy (AM) and X-ray Diffraction (XRD) confirmed bastnäsite and monazite as the dominant REE-bearing minerals. Quantitative Rietveld refinement on the highly enriched fractions provided further evidence, confirming a substantial increase in the weight percentage of bastnäsite with decreasing particle size.

The combined AM and XRD results provided a comprehensive understanding of the mineral associations, highlighting a strong affinity of REE-bearing phases with barite and iron oxides rather than the dominant phase fluorite. Furthermore, hydrometallurgical leaching experiments demonstrated the direct process significance of these findings. The highest leachate concentrations of the most prevalent REE (La, Ce, Nd) were obtained from the finest particle fractions where REE minerals are more readily accessible for leaching as evident from AM results whereas they are found as encapsulated in coarser particles resulting decrease in concentration. Additionally, the leaching efficiency was found to be largely consistent, regardless of the acid medium chosen (HNO_3 or H_2SO_4), simplifying flowsheet selection. It should be noted that this study focuses on the characterization and direct leaching of calcined ore fractions. Physical beneficiation methods such as flotation as well as the optimization of comminution circuits, are outside the scope of this work and remain subjects for future investigations to further enhance REE recovery.

In conclusion, the data presented herein confirms that particle size is the governing control parameter for both the enrichment and subsequent successful hydrometallurgical recovery of REE from Kızılcaören deposit. The rigorous, size-dependent methodology utilized in this study provides a vital, reproducible framework not only for optimizing the energy-efficient processing flowsheet for this strategic Turkish resource but also for guiding the technological development of other similar complex, bastnäsite-type REE ores globally.

Declaration of generative AI and AI-assisted technologies in the writing process

During the preparation of this work, the authors used different public ai tools (Chatgpt, and Gemini) just in order to increase the readability of the paper. After using this tool, the authors reviewed and edited the content as needed and take full responsibility for the content of the published article.

CRediT authorship contribution statement

S. Samet Kaplan: Writing – original draft, Visualization, Investigation. **Cisem Celik-Kurtulan:** Writing – original draft, Investigation. **Elif Emil-Kaya:** Writing – review & editing, Investigation, Conceptualization. **Gabriella Tranell:** Writing – review & editing, Supervision, Funding acquisition, Conceptualization. **M. Seref Sonmez:** Writing – review & editing, Supervision, Funding acquisition, Conceptualization.

Declaration of competing interest

The authors declare that they have no known competing financial interests or personal relationships that could have appeared to influence the work reported in this paper.

Acknowledgments

Authors would like to acknowledge that this study is financially supported by Turkish Energy, Nuclear and Mineral Research Agency–Rare Earth Elements Research Institute (TENMAK-NATEN) (Project No: A2.H1.P20), and Istanbul Technical University BAP division (Project No: MDK-2022–43727). The Research Council of Norway is acknowledged for the support to the Norwegian Laboratory for Mineral and Materials Characterisation, MiMaC, project number 269842/F50. Also, we would like to thank to ITU-MEMTEK research center for their help for conducting SEM-EDX analysis. This paper is submitted in partial fulfillment of PhD degree at Istanbul Technical University.

Supplementary materials

Supplementary material associated with this article can be found, in the online version, at doi:10.1016/j.rineng.2026.108961.

Data availability

Data will be made available on request.

References

[1] European Commission, Critical raw materials factsheets (2020), 2020. https://doi.org/10.2873/92480.
[2] Z.Y. Wang, H.R. Fan, L. Zhou, K.F. Yang, H.D. She, Carbonatite-related REE deposits: an overview, Minerals 10 (2020) 1–26, https://doi.org/10.3390/min10110965.
[3] D. Guo, Y. Liu, Occurrence and geochemistry of bastnäsite in carbonatite-related REE deposits, Mianning–Dechang REE belt, Sichuan Province, SW China, Ore Geol. Rev. 107 (2019) 266–282, https://doi.org/10.1016/j.oregeorev.2019.02.028.
[4] J. Zhou, X. Wang, L. Nie, J.M. McKinley, H. Liu, B. Zhang, Z. Han, Geochemical background and dispersion pattern of the world's largest REE deposit of Bayan Obo, China, J. Geochem. Explor. 215 (2020) 106545, https://doi.org/10.1016/J.GEXPLO.2020.106545.
[5] M. Deng, C. Xu, W. Song, H. Tang, Y. Liu, Q. Zhang, Y. Zhou, M. Feng, C. Wei, REE mineralization in the Bayan Obo deposit, China: evidence from mineral paragenesis, Ore Geol. Rev. 91 (2017) 100–109, https://doi.org/10.1016/j.oregeorev.2017.10.018.
[6] U.S. Geological Survey, Mineral commodity summaries, US Dep. Inter. (2025), https://doi.org/10.3133/mcs2025.
[7] R. Neumann, E.B. Medeiros, Comprehensive mineralogical and technological characterisation of the Araxá (SE Brazil) complex REE (Nb-P) ore, and the fate of its processing, Int J Min. Process 144 (2015) 1–10, https://doi.org/10.1016/j.minpro.2015.08.009.
[8] A.L. Giovannini, R.H. Mitchell, A.C. Bastos Neto, C.A.V. Moura, V.P. Pereira, C. G. Porto, Mineralogy and geochemistry of the Morro dos Seis Lagos siderite carbonatite, Amazonas, Brazil, Lithos. 360–361 (2020) 105433, https://doi.org/10.1016/j.lithos.2020.105433.
[9] T.K.D. Nhu, V.L. Pham, T.C. Vu, V.D. Tran, An overview of rare earth ores beneficiation in vietnam, Inż. Miner. 1 (2021), https://doi.org/10.29227/IM-2021-02-20.
[10] Q. Van Phan, T.T. Dao, P. Nguyen, D.H. Trinh, An assessment of natural radioactivity in the Namxe Rare Earth Deposit, Laichau Province, Vietnam, Minerals 9 (2019) 602, https://doi.org/10.3390/min9100602.
[11] N.D. Chau, P. Jadwiga, P. Adam, D. Van Hao, L.K. Phon, J. Paweł, General characteristics of rare earth and radioactive elements in Dong Pao deposit, Lai Chau, Vietnam, Vietnam J. Earth Sci. 39 (2017) 14–26, https://doi.org/10.15625/0866-7187/39/1/9181.
[12] G.A. Moldoveanu, V.G. Papangelakis, Recovery of rare earth elements adsorbed on clay minerals: I. Desorption mechanism, Hydrometallurgy 117–118 (2012) 71–78, https://doi.org/10.1016/J.HYDROMET.2012.02.007.
[13] L. Ding, G. Azimi, Impact of particle size and associated minerals on rare earth desorption and incorporation mechanisms in a South American ion-adsorption clay, Sci. Rep. (2024) 16216, https://doi.org/10.1038/s41598-024-67134-2, 2024 14:1 14-.
[14] V.V. Seredin, S. Dai, Coal deposits as potential alternative sources for lanthanides and yttrium, Int. J. Coal. Geol. 94 (2012) 67–93, https://doi.org/10.1016/J.COAL.2011.11.001.
[15] R.K. Taggart, J.C. Hower, G.S. Dwyer, H. Hsu-Kim, Trends in the rare earth element content of U.S.-based coal combustion fly ashes, Env. Sci Technol 50 (2016) 5919–5926, https://doi.org/10.1021/ACS.EST.6B00085.
[16] A. Kolker, C. Scott, J.C. Hower, J.A. Vazquez, C.L. Lopano, S. Dai, Distribution of rare earth elements in coal combustion fly ash, determined by SHRIMP-RG ion microprobe, Int. J. Coal. Geol. 184 (2017) 1–10, https://doi.org/10.1016/J.COAL.2017.10.002.
[17] G. Harshitha, I. González-Álvarez, C. Manikyamba, J. D'Andres, J.K. Yadav, M. K. Mukherjee, Critical mineral potential of Indian phosphorites: evidence of REE enrichment in Ediacaran sediments from the Cuddapah Basin, J. Geochem. Explor. 280 (2026) 107918, https://doi.org/10.1016/J.GEXPLO.2025.107918.
[18] S. Ferhaoui, R. Kechiched, O. Bruguier, R. Sinisi, L. Kocsis, G. Mongelli, D. Bosch, O. Ameur-Zaimeche, R. Laouar, Rare earth elements plus yttrium (REY) in

phosphorites from the Tébessa region (Eastern Algeria): abundance, geochemical distribution through grain size fractions, and economic significance, J. Geochem. Explor. 241 (2022) 107058, https://doi.org/10.1016/J.GEXPLO.2022.107058.
[19] R. Aouachria, R. Kechiched, R. Buccione, G. Mongelli, O. Ameur-Zaimeche, O. Bruguier, L. Kocsis, R. Laouar, Geochemistry and economic evaluation of REE + Y potential in the fine-grained matrix of sedimentary phosphorites from the Tebessa region, eastern Algeria, J. Geochem. Explor. 280 (2026) 107889, https://doi.org/10.1016/J.GEXPLO.2025.107889.
[20] H. Kaplan, Eskişehir - Sivrihisar • kızılcaören Köyü Yakın Güneyi «Nadir Toprak Elementleri ve Toryum Kompleks Cevher Yatağı, Jeol. Mühendisliği Derg. 1 (1977) 29–34.
[21] H. Öztürk, S. Altuncu, N. Hanilçi, C. Kasapçı, K.M. Goodenough, Rare earth element-bearing fluorite deposits of Turkey: an overview, Ore Geol. Rev. 105 (2019) 423–444, https://doi.org/10.1016/j.oregeorev.2018.12.021.
[22] F. Pirajno, T. Ünlü, C. Dönmez, M.B. Şahin, Mineral Resources of Turkey, Springer International Publishing, Cham, 2019, https://doi.org/10.1007/978-3-030-02950-0.
[23] A.H. Gültekin, Y. Örgün, The Kızılcaören Fluorite-Barite-REE Deposits Associated With Tertiary Alkaline Volcanics, 1, Anadolu Üniversitesi Bilim ve Teknoloji Dergisi A - Uygulamalı Bilimler ve Mühendislik, Sivrihisar, Eskişehir, 2000, pp. 85–94.
[24] A.H. Gültekin, Y. Örgün, F. Suner, Geology, mineralogy and fluid inclusion data of the Kizilcaören fluorite–barite–REE deposit, Eskisehir, Turkey, J. Asian Earth. Sci. 21 (2003) 365–376, https://doi.org/10.1016/S1367-9120(02)00019-6.
[25] G. Turker, K. Delice, A. Temizkalb, O.C. Ozgur, B.S. Sozer, Beneficiation of Eskişehir Beylikova Bastnasite ore and rare earth elements recovery, in: Materials Proceedings, RawMat 2023, Multidisciplinary Digital Publishing Institute, 2023, p. 44, https://doi.org/10.3390/MATERPROC2023015044.
[26] M. Camalan, A. Temizkalb, M. Gülsün Kılıç, E.C. Orhan, Ş.L. Ergün, E. Gülcan, Characterisation of a Turkish rare earth ore to asses the enrichment potential, in: 17th International Mineral Processing Symposium, Istanbul, 2022, pp. 915–920.
[27] N. Yeşilören-Görmüş, G. Gürtekin, A. Erdem, A. Gülmez, Determination of minerals containing rare earth elements (REE) in Kızılcaören (Sivrihisar) region using mineral liberation analysis (MLA) method, Int. J. Pure Appl. Sci. 7 (2021) 251–264, https://doi.org/10.29132/ijpas.907212.
[28] E. Baştürkcü, C. Şavran, A.E. Yüce, S.İ. Timur, Revealing the effects of mechanical attrition applied on Eskisehir-Beylikova REE ore utilizing MLA, Min. Eng 186 (2022) 107733, https://doi.org/10.1016/J.MINENG.2022.107733.
[29] S.S. Kaplan, C.C. Kurtulan, S. Gurmen, G. Orhan, M.S. Sonmez, Influence of calcination conditions on deep eutectic solvents (DES) leaching efficiency of light rare earth elements in bastnasite ore, Min. Eng 220 (2025), https://doi.org/10.1016/j.mineng.2024.109087.
[30] Y. Ni, J.E. Post, J.M. Hughes, The crystal structure of parisite-(Ce), Ce2CaF2(CO3) 3, Am. Mineral. 85 (2000) 251–258, https://doi.org/10.2138/am-2000-0126.